



F3

**Faculty of Electrical Engineering
Department of Cybernetics**

Bachelor's Thesis

Fusion of UWB-Based Distance Sensors with a Visual Relative Localization System

Vít Petřík

**Supervisor: Ing. Viktor Walter
Study program: Cybernetics and Robotics
May 2023**

I. Personal and study details

Student's name: **Petřík Vít** Personal ID number: **499246**
Faculty / Institute: **Faculty of Electrical Engineering**
Department / Institute: **Department of Cybernetics**
Study program: **Cybernetics and Robotics**

II. Bachelor's thesis details

Bachelor's thesis title in English:

Fusion of UWB-Based Distance Sensors with a Visual Relative Localization System

Bachelor's thesis title in Czech:

Fúze senzoru vzdálenosti na báze UWB se systémem vizuální relativní lokalizace

Guidelines:

Range sensors based on the UWB (Ultra-wideband) signal technology enable robust wireless measurement of relative distance between two devices. This property complements the drawbacks of relative localization based on computer vision, such as the UVDAR system used by the MRS group, namely their reduced precision in terms of distance estimation. Compared to UWB sensors however, computer vision methods make it possible to estimate the relative bearing of a target.

If used together, the two sensor types can enable a more precise relative localization of flying Unmanned Aerial Vehicles (UAVs) than if each was used separately.

The goal of this thesis is to develop a system for fusion of the output data from the two aforementioned sensor types, and to implement this system in the Robot Operating System (ROS).

The system should optionally also be tested on real flying UAV.

Bibliography / sources:

- [1] V. Walter, N. Staub, A. Franchi and M. Saska. UVDAR System for Visual Relative Localization With Application to Leader-Follower Formations of Multirotor UAVs. IEEE Robotics and Automation Letters 4(3):2637-2644, July 2019.
- [2] Y. Shimizu and Y. Sanada, "Accuracy of relative distance measurement with ultra wideband system," IEEE Conference on Ultra Wideband Systems and Technologies, 2003, 2003, pp. 374-378, doi: 10.1109/UWBST.2003.1267867.
- [3] Stanford Artificial Intelligence Laboratory et al. (2018). Robotic Operating System. Retrieved from <https://www.ros.org>

Name and workplace of bachelor's thesis supervisor:

Ing. Viktor Walter Multi-robot Systems FEE

Name and workplace of second bachelor's thesis supervisor or consultant:

Date of bachelor's thesis assignment: **20.02.2023** Deadline for bachelor thesis submission: **26.05.2023**

Assignment valid until: **22.09.2024**

Ing. Viktor Walter
Supervisor's signature

prof. Ing. Tomáš Svoboda, Ph.D.
Head of department's signature

prof. Mgr. Petr Páta, Ph.D.
Dean's signature

III. Assignment receipt

The student acknowledges that the bachelor's thesis is an individual work. The student must produce his thesis without the assistance of others, with the exception of provided consultations. Within the bachelor's thesis, the author must state the names of consultants and include a list of references.

Date of assignment receipt

Student's signature

Acknowledgements

It is a privilege for me to extend my heartfelt appreciation to my supervisor, Ing. Viktor Walter, whose unwavering support and guidance have been instrumental in assisting me throughout my work. I am profoundly grateful to the CTU MRS group for granting me the invaluable opportunity to collaborate with their cutting-edge UAV platform.

Without the unwavering support of my family, who consistently provided me with a secure haven, I would have been unable to complete this thesis. I am deeply appreciative of the invaluable interactions I had with my fellow students and colleagues at Siemens Advanta, as they provided me with the opportunity to engage in insightful discussions pertaining to the technical aspects of my thesis.

Declaration

I declare that the presented work was developed independently and that I have listed all sources of information used within it in accordance with the methodical instructions for observing the ethical principles in the preparation of university theses.

Prague, 26. May 2023
signature

Abstract

For the operation of multi-robot systems, it is crucial that each robot possesses information about the whole system. This information could be GNSS coordinates shared through multiple robots. This approach, however, falls apart when the system needs to operate indoors or when the precision of GNSS is not sufficient. One solution is to equip the space with a motion capture system, but it is not always a viable solution. A popular solution for such a problem is to employ visual relative localizations.

This thesis explores one of the possible paths to improve measurements from relative visual localizations. A proposed solution for this task is a sensor based on Ultra-wideband technology. As our experiments show, the solution offers high precision and low latency localization of multiple robots.

Keywords: UAV, UWB, ROS, simulation, Gazebo, Unmanned copter, data fusion, ultra-wide band, relative mutual localization, Kalman filter, unscented kalman filter

Supervisor: Ing. Viktor Walter
Czech Technical University
Faculty of Electrical Engineering
Department of Cybernetics
Karlovo náměstí 13
121 35 Prague 2
Czech Republic

Abstrakt

Pro provoz multirobotických systému je důležité, aby každý robot měl informaci o celém systému. Tato informace může být zprostředkovaná sdílením GNSS souřadnic mezi roboty. Bohužel tento přístup nelze aplikovat v prostředích bez příjmu GNSS nebo v aplikacích, kde je přesnost GNSS příliš nízká. Jedna z možností je takovéto prostředí vybavit systémem snímání pohybu pomocí kamer, ale toto není vždy možné. Částečným řešením pro tyto problémy je využití vizuální relativní lokalizace.

Tato bakalářská práce zkoumá jednu z možností, jak vylepšit přesnosti vizuální relativní lokalizace. Navrhnuté řešení spočívá ve slučování dat ze systému vizuální relativní lokalizace s ultraširokopásmovým rádiiem pro měření vzdálenosti. Provedené experimenty ukazují, že navrhnuté řešení umožňuje přesnou relativní lokalizace několika robotů bez znatelného zpoždění.

Klíčová slova: fúze dat, ultraširokopásmová technologie, UWB, ROS, UAV, simulace, bezpilotní koptéra, Gazebo, relativní vzájemná lokalizace, počítačové vidění, kalmánův filtr

Překlad názvu: Fúze senzoru vzdálenosti na báze UWB se systémem vizuální relativní lokalizace

Contents

1 Introduction	1	4.2 Extended Kalman filter	19
1.1 State of the art	2	4.3 Unscented Kalman filter	20
1.2 Ranging and positioning in Civil Aviation	2	5 UAV implementation	23
En-route positioning and navigation	2	5.1 Qorvo DW1000 UWB PHY radio	23
Aircraft-to-Aircraft positioning	3	5.2 Object tracker	25
2 Ultra-violet Direction and Ranging	5	6 Simulations and real-world experiments	29
3 Ultra-wide band	7	6.1 Ultra-wide band experiments . . .	29
3.1 MAC layer	8	Line segment test	29
3.2 Physical Layer	8	Circular trajectory	29
PPDU format	9	Results	30
Symbol structure	11	6.2 UVDAR and UWB fusion experiments	31
3.3 Ranging techniques	13	Leader follower algorithm	31
Time Difference of Arrival	13	Results	31
Two-way ranging	14	7 Conclusion	35
4 Kalman filters	17	References	37
4.1 Linear Kalman filter	18	A Source code	41

B ISO-OSI network model 43

**C Object tracker and UWB
evaluation tests** 45

Figures

2.2 UVDAR processing data flow.	5	5.1 System overview.	24
2.1 Image from UV camera with extracted bright spots.	6	5.2 Qorvo DWM1001 development board.	25
2.3 Geometry of UAV position calculation with 3 visible markers. [23]	6	5.3 Structure of ranging message. Numbers denote bytes.	25
3.1 MAC frame format. [4]	8	5.4 Fuse of UVDAR and UWB measurements using Kalman filters.	26
3.2 Data flow according to. [2]	9	5.5 Situational schema of data fusion.	27
3.3 PPDU encoding process. [2]	10	5.6 Measurement function for fusing distance.	27
3.4 SHR field structure. [4]	10	6.1 Holybro X500 with UVDAR cameras and UWB radio.	30
3.5 PHR field structure. [4].	11	6.2 Circular trajectory experiment.	31
3.6 Symbol structure. [4]	11	6.3 Transfer characteristic of UWB.	32
3.7 Example of BPM-BPSK modulation,	12	6.4 Trajectory plotted in time with error.	33
3.8 Reference pulse of UWB radio.	13	6.5 Comparison between different radiation angles.	33
3.9 Two way ranging with two round trips.	15	6.6 Visual representation of the leader-follower algorithm.	34
4.1 Comparison between sampling, EKF and sigma points. [13]	20	6.7 Leader-follower algorithm results.	34
		B.1 OSI-ISO network model.	43

C.1 Screenshot from Gazebo simulator showing the two UAVs.	45
C.2 Circle path with UWB fusion.	46
C.3 Circle path with standalone UVDAR.	47
C.4 Square path with UWB fusion.	48
C.5 Square path with UWB fusion.	49
C.6 Flower path with UWB fusion.	50
C.7 Flower path with standalone UVDAR.	51
C.8 Test of not moving UWBs.	52

Tables

3.1 The duration of the reference pulse for each channel. [2]	12
---	----



Chapter 1

Introduction

In recent years, the use of unmanned aerial vehicles (UAVs) has been rapidly growing due to their versatility and wide range of applications, from aerial photography and surveillance to delivery services ¹ and search and rescue operations [14]. The problem of relative localization in UAV swarms is a critical challenge in enabling cooperative behavior and avoiding collisions.

To address this problem, a novel system is proposed in this thesis that combines computer vision and ultra-wideband (UWB) technology for direction and range measurements, respectively. By combining these measurements with a Kalman filter, the relative positions and orientations of UAVs can be estimated with high accuracy, even in GNSS-denied environments such as buildings or underground areas [14]. This approach has a significant advantage over existing methods, which often rely on GNSS [20] or motion capture ² and are therefore limited in their ability to operate in challenging environments or without additional infrastructure onsite.

This thesis addresses designing and implementing an effective relative localization system for UAV swarms using computer vision and UWB technology and evaluates how well it performs in real-world scenarios. First, a review of the proposed system and its key components, including the computer vision algorithms for direction estimation and the UWB hardware for range measurement, will be presented. Finally, the performance of the system will be evaluated through a series of experiments in both simulated and real-world environments.

By developing and testing this system, a contribution will be made to the growing body of research on multi-robot systems and pave the way for new applications of UAV swarms in challenging environments.

¹Blood and packages delivery <https://www.flyzipline.com>

²Motion capture OptiTrack <https://optitrack.com>

1.1 State of the art

Extensive research has already been conducted on the utilization of Ultra-Wideband (UWB) technology in Unmanned Aerial Vehicle (UAV) applications. Majority of published articles primarily concentrate on the implementation of UWB technology using an architecture based on UWB anchors [9,18]. Nevertheless, this particular implementation is unsuitable for deployment in potentially hazardous environments, particularly for search and rescue applications. Article *Decentralized Visual-Inertial-UWB Fusion for Relative State Estimation of Aerial Swarm* [26] proposes system architecture and the fusion algorithm, which combines visual-inertial odometry (VIO) and UWB ranging measurements in a tightly-coupled manner. However, this approach would be ineffective in environments lacking distinct features.

Hence, the subsequently proposed system stands out for its exceptional ease of deployment, accuracy of measurements and the robustness it offers.

1.2 Ranging and positioning in Civil Aviation

Along with the widely adopted localization and navigation via GNSS, aviation has developed several ranging and positioning solutions that can be analyzed and used to take a cue from for utilization in UAV applications.

En-route positioning and navigation

DME (Distance Measuring Equipment) is a type of radio navigation equipment that provides an accurate slant range from the aircraft to selected ground-based DME station. The DME uses the transmission of UHF band radio signals between aircraft and ground station on the principle of two-way ranging [1]. DME consists of ground transponders and aircraft on-board avionics. Aircraft DME avionics first interrogate ground transponders, and the transponder replies back to avionics through a pair of pulses. The time elapsed from the interrogation to the receipt of the replies from the ground transponder is measured and when the internal processing delay of the ground equipment computer is known, a distance representing slant range between aircraft and the ground station can be determined [8].

Over the time, DME has become an indispensable component of air traffic positioning and navigation during various phases of flight including departure, en-route flight, approach, landing or even missed approach procedure [6]. It often works as a complement to other systems such as VOR, ILS or MLS, further increasing its versatility. With advancements in technology, the latest generation of DME transponders surpass the outdated operational standards, delivering improved navigational performance in accordance with specification required by Performance Based Navigation (PBN) standard of International Civil Aviation Organization (ICAO).

■ Aircraft-to-Aircraft positioning

The aviation in general prides itself on a reputation of safe and well managed mean of transport with use of state-of-the-art equipment, procedures and training. Besides other safety related aspects, the aircraft-to-aircraft separation is a crucial when navigating the aircraft along the flight route from the very beginning of the flight till disembarking at the destination.

Development and incorporation of the Traffic Alert and Collision Avoidance System (TCAS) in the late 1980s into the aircraft systems serves as an effective solution to mitigate the risk of midair collisions between individual aircraft [19].

TCAS is a current implementation of the ICAO Airborne Collision Avoidance System (ACAS) technical standard and is a family of airborne devices that operate autonomously, independently from the ground-based air traffic control (ATC) and are designed to offer collision avoidance protection [7,19]. The concept of TCAS comprises of specialized TCAS computer unit and simultaneously takes advantage of already existing on-board equipment, the transponder of secondary surveillance radar installed on aircraft for ground ATC purposes and provides no protection against an aircraft, that does not possess an operating transponder [16].

Chapter 2

Ultra-violet Direction and Ranging

The Ultra-violet Direction and Ranging (UVDAR) system, developed by the esteemed Multi-robot system group at CTU [23], revolutionizes relative localization through the implementation of computer vision techniques. Comprised of active UV LED markers (395nm) and an industrial-grade camera (mvBlueFOX MLC200wG) equipped with a UV bandpass filter and fisheye lens, UVDAR excels at accurately distinguishing active markers from the background. This exceptional capability enables the system to operate effectively under diverse lighting conditions, ensuring reliable performance. For a visual representation of the UVDAR system, refer to Figure 2.1, which provides an example view captured by the camera with extracted bright spots.

Figure 2.2 presents a comprehensive overview of the UVDAR system, showcasing its data flow and functionality.

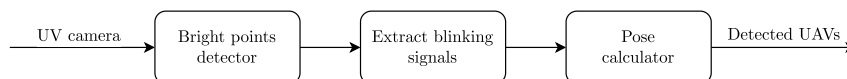


Figure 2.2: UVDAR processing data flow.

The *bright points detector* step uses Features from accelerated segment test (FAST) algorithm to extract the UV markers. The FAST algorithm is a method for detecting corners in images, which are useful for tracking and mapping objects in 3D model-based tracking systems. It was introduced by Edward Rosten and Tom Drummond in 2005 [15]. It uses a 16-pixel circle around a candidate point and compares the intensity of the pixels with a threshold to determine if the point is a corner. It also uses a high-speed test and machine learning techniques to improve the performance and accuracy of the corner detection [15]. The FAST algorithm can perform full-frame real-time feature detection and can handle large prediction errors and rapid movements [15]. The implementation of the FAST algorithm can distinguish sun and UV markers, as the sun is a major UV light source. Recently great

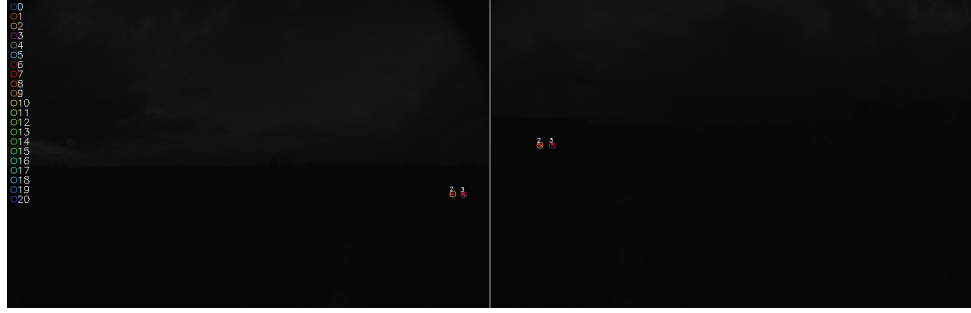


Figure 2.1: Image from UV camera with extracted bright spots.

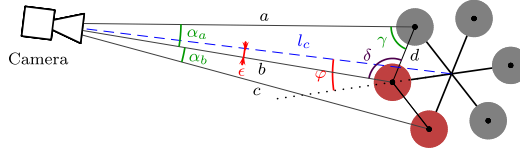


Figure 2.3: Geometry of UAV position calculation with 3 visible markers. [23]

effort was made by MRS group to implement FAST using GPU resources to offload CPU.

The *extract blinking signals* step uses 4D hough transformation to evaluate the blinking frequency of the UV LED marker. The step involves buffering the extracted bright points as *t-points* $[x \ y \ t]$ from multiple frames and processing them by the Hough transformation [22]. The Hough transformation is used to approximate the motion of *t-points* with *t-lines*. The presence of *t-points* within *t-lines* is used to match a blinking signal with a predefined sequence ID.

The *pose calculator* will perform the final result, as it can assign the retrieved markers to a physical UAV model, estimate its position, orientation and covariance matrix. Figure 2.3 provides a visual representation of the geometric interpretation involved in the pose calculation process.

Chapter 3

Ultra-wide band

The following chapter will introduce the ultra-wide band according to IEEE 802.15.4 [2]. Another definition exists by Federal Communications Commission (FCC), but it will not be discussed in this thesis.

To fully understand what ultra-wide band means it is necessary to define what bandwidth means by equation 3.1 and what center frequency means by equation 3.2.

$$\text{bandwidth}_{-3\text{dB}} = f_{\text{max}} - f_{\text{min}} \quad (3.1)$$

$$f_{\text{center}} = \frac{f_{\text{max}} - f_{\text{min}}}{2} = f_{0\text{db}} \quad (3.2)$$

The ultra-wide band radio uses a bandwidth of 500 Mhz and more. This fact provides UWB with its unique ranging capabilities. The *IEEE 802.15.4 Low-Rate Wireless Personal Area Networks* [2] specifies the physical and data link layers of the ISO-OSI network model B.1.

Today, UWB is mainly used in consumer electronics¹ or in manufacturing plants to track assets, ground vehicles and people²³.

¹Apple AirTag <https://www.apple.com/airtag/>

²Siemens RTLS <https://www.siemens.com/global/en/products/automation/industrial-identification/simatic-rtls.html/>

³Sewio real-time location system <https://www.sewio.net/>

Bytes: 2	1	0/2	0/2/8	0/2	0/2/8	0/5/6/10/14	variable	2
Frame Control	Sequence Number	Destination PAN Identifier	Destination Address	Source PAN Identifier	Source Address	Auxiliary Security Header	Frame Payload	FCS
		Addressing fields						
MHR							MAC Payload	MFR

Figure 3.1: MAC frame format. [4]

3.1 MAC layer

IEEE 802.15.4 describes the MAC layer for low-rate wireless personal networks, including UWB. The MAC layer is responsible for coordinating access to the shared wireless channel, managing network associations and disassociations, and providing security and reliability features. The MAC layer inserts an MAC header and an MAC footer before and after a network-layer frame, respectively. The MAC header contains information such as frame type, source and destination addresses, sequence number, and security parameters. The MAC footer contains a CRC check. The IEEE 802.15.4 MAC layer supports two modes of operation: beacon-enabled and non-beacon-enabled. In beacon-enabled mode, a coordinator device periodically broadcasts beacons to synchronize devices on its network and allocate contention-free periods for data transmission. In non-beacon-enabled mode, devices use a slotted or unslotted carrier sense multiple access with collision avoidance (CSMA-CA) mechanism to access the channel. The exact layout of the MAC frame format is described in figure 3.1.

3.2 Physical Layer

The physical layer (PHY) of the UWB was described in IEEE 802.15.4-2011 [2] as the UWB PHY. Later in IEEE 802.15.4-2015 [4] the PHY was named High repetition pulse (HRP) UWB PHY. This decision was made due to the introduction of Low repetition pulse (LRP) UWB PHY. Only the HRP UWB PHY will be discussed. The standard defines three operation bands:

- sub-gigahertz band consisting of a single channel spectrum from 249.6 MHz to 749.6 MHz.
- Low band with spectrum from 3.1 GHz to 4.8 GHz.
- High band with spectrum from 6 GHz to 10.6 GHz.

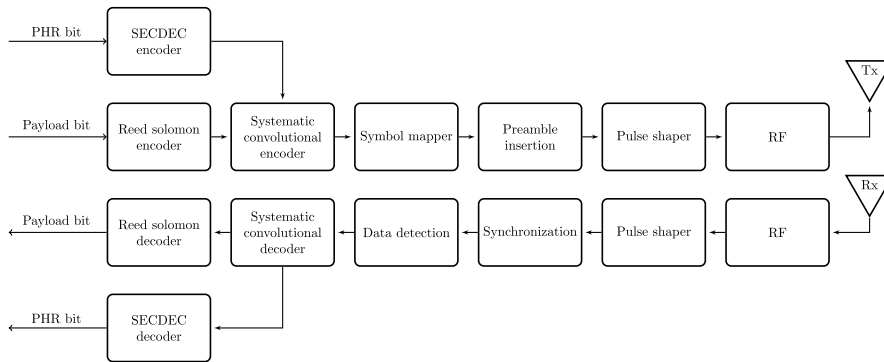


Figure 3.2: Data flow according to. [2]

The PHY uses an impulse radio signaling scheme with band-limited pulses and supports high data rates and precise ranging applications. It also uses a combination of burst position modulation (BPM) and binary phase-shift keying (BPSK) to modulate symbols. The overview of the physical layer is shown in figure 3.2.

■ PPDU format

Each physical layer protocol data unit (PPDU) consists of a preamble, PHY header, and the data itself. The process of encoding the whole PPDU can be seen in figure 3.3.

Reed-Solomon encoding is used to encode the physical service data unit (PSDU) of the HRP UWB PHY. It adds redundant symbols to the original message symbols to form a codeword that can be decoded using polynomial interpolation or factorization techniques. Reed-Solomon encoding improves the error-correction performance of the HRP UWB PHY and enables it to handle burst errors or random errors that may occur in the wireless channel⁴.

Convolutional encoding is used to encode the PSDU of the HRP UWB PHY after Reed-Solomon encoding. It uses a finite state machine with memory cells to generate output bits based on the current and previous input bits.

⁴Mathworks HRP UWB IEEE 802.15.4a/z Waveform Generation <https://www.mathworks.com/help/comm/ug/hrp-uw-ieee-802.15.4z-waveform-generation.html>

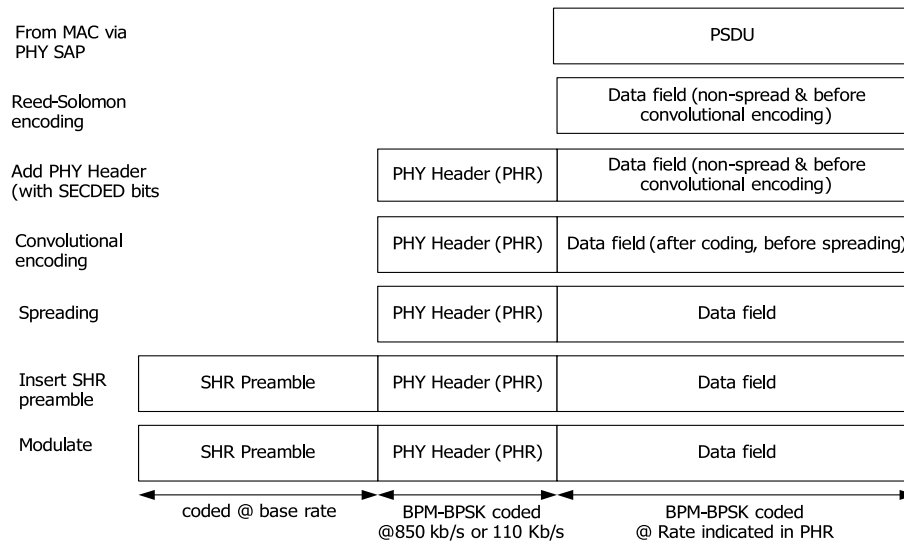


Figure 3.3: PPDU encoding process. [2]

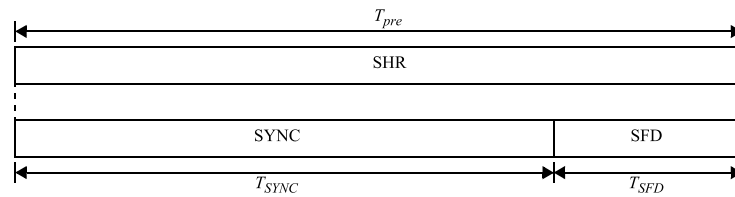


Figure 3.4: SHR field structure. [4]

It adds parity bits to the original information bits to form a codeword that can be decoded using the Viterbi algorithm or other sequential decoding techniques. Convolutional encoding improves the error correction performance of the HRP UWB PHY and enables it to handle noisy or fading channels.

A preamble in HRP UWB PHY is a sequence of known bits sent at the beginning of each frame. It is used for frame synchronization, channel estimation, and ranging measurements. It consists of two parts: a synchronization header (SHR) 3.4 and a physical layer header (PHR) 3.5.

The SHR contains a preamble symbol (SYNC) and a start-of-frame delimiter (SFD). The SFD is a fixed sequence of pulses that indicates the start of a frame. The PS is a burst of UWB pulses that can be modulated by burst position modulation (BPM) or binary phase-shift keying (BPSK). The preamble symbol repetitions (PSR) define the number of repeated sequences, ranging from 16 to 4,096 repetitions.

Bits: 0–1	2–8	9	10	11–12	13–18
Data Rate	Frame Length	Ranging	Reserved	Preamble Duration	SECDED

Figure 3.5: PHR field structure. [4]

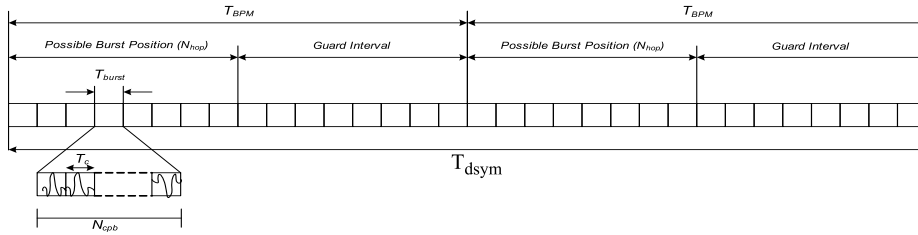


Figure 3.6: Symbol structure. [4]

The PHR contains information about the data to be received, including the length of the data and the data rate used to transmit the data. It also contains additional information elements to facilitate ranging information exchange.

■ Symbol structure

A symbol is the basic unit of information in the HWP UWB PHY. It consists of a short burst of UWB pulses that lasts for 2 ns and occupies a bandwidth of 0.5-1.3 GHz. The burst can be placed in one of the two possible burst intervals, and its phase can be inverted or not, as can be seen in Figure 3.6. These two choices allow each symbol to carry two bits of information using burst position modulation (BPM) and binary phase-shift keying (BPSK); an example of the modulation can be found in figure 3.7.

The burst hopping position is a parameter that determines the time position of the UWB pulses within a burst interval. Scrambling code is a pseudo-random sequence that is applied to the data bits before modulation. It is used to randomize the data bits and reduce the peak-to-average power ratio (PAPR) of the UWB pulses.

IEEE defines the reference pulse as a root-raised cosine pulse with roll-off factor $\beta = 0.5$ 3.3.

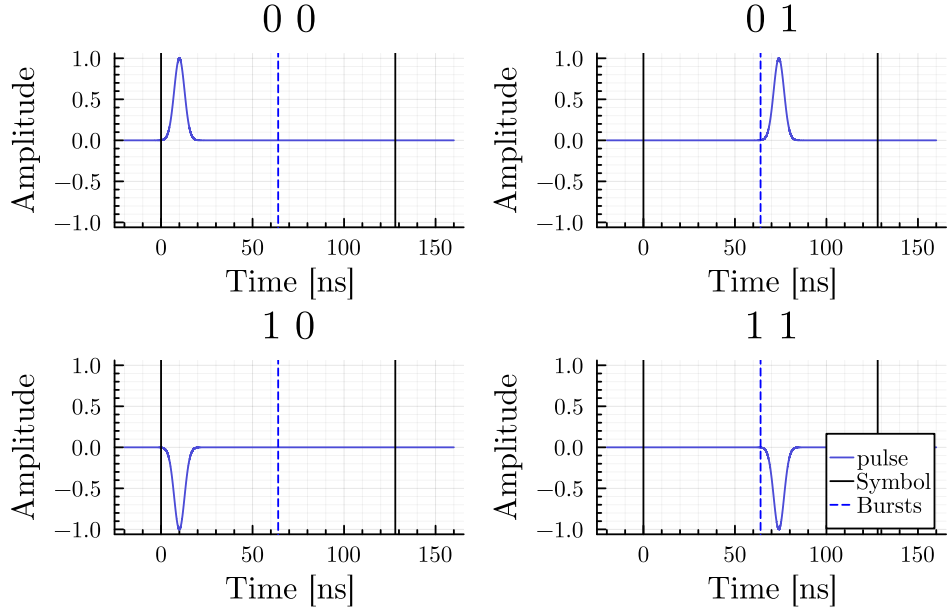


Figure 3.7: Example of BPM-BPSK modulation,

$$r(t) = \frac{4\beta}{\pi\sqrt{T_p}} \frac{\cos[(1+\beta)\pi t/T_p] + \frac{\sin[(1-\beta)\pi t/T_p]}{4\beta(t/T_p)}}{1 - (4\beta t/T_p)^2} \quad (3.3)$$

The parameter T_p stands for the duration of the pulse. The duration is defined for each channel by table 3.1.

Channel number	Pulse duration T_p (ns)	Main lobe width T_w (ns)
{0:3, 5:6, 8:10, 12:14}	2.00	0.5
7	0.92	0.2
{4, 11}	0.75	0.2
15	0.74	0.2

Table 3.1: The duration of the reference pulse for each channel. [2]

Figure 3.8 further illustrates a waveform of the pulse. However, an actual hardware system cannot fully realize the shape of the reference pulse. Therefore IEEE 802.15.4 constrains the transmitted pulse $p(t)$ by a cross-correlation function 3.4 where E_r is the energy of $r(t)$ and E_p is the energy of $p(t)$.

$$\phi(\tau) = \frac{1}{\sqrt{E_r E_p}} \text{Re} \int_{-\infty}^{\infty} r(t) p(t - \tau) dt \quad (3.4)$$

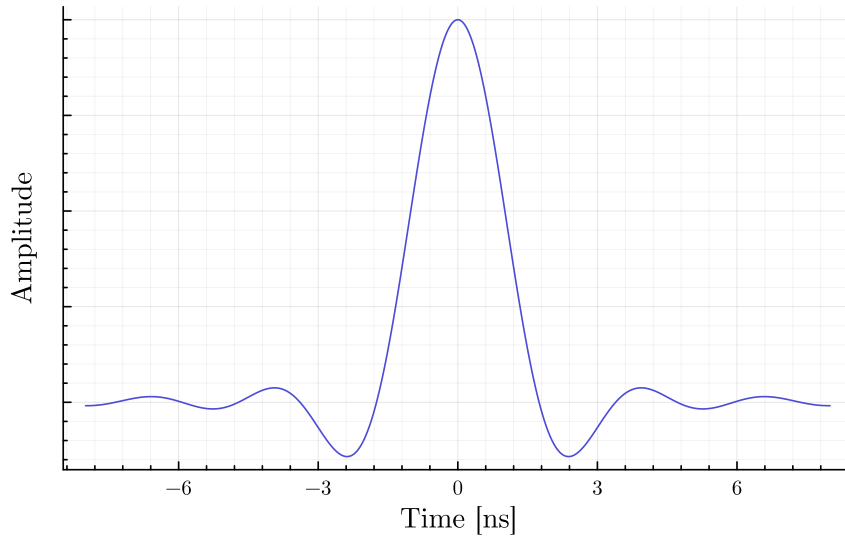


Figure 3.8: Reference pulse of UWB radio.

For PHY to be IEEE compliant, the main lobe of the transmitted pulse must have a magnitude of cross correlation $|\phi(\tau)|$ at least 0.8, and the magnitude of the sidelobes must not be greater than 0.3.

■ 3.3 Ranging techniques

■ Time Difference of Arrival

Time difference of arrival (TDOA) position estimation is a technique that uses the difference in the arrival times of UWB signals at multiple receivers to estimate the position of a transmitter.

TDOA position estimation requires at least four receivers and one transmitter for 3D localization. The receivers measure the time of arrival (TOA) of the UWB signals. The TOA measurements are then used to calculate the TDOA values between different pairs of receivers [27].

$$\sqrt{\mathbf{x}_r^T \hat{\mathbf{x}}} - \sqrt{\mathbf{x}_i^T \hat{\mathbf{x}}} = c(t_r - t_i) \quad (3.5)$$

Where:

- $\hat{\mathbf{x}}$ = estimated position of the transmitter.
- \mathbf{x}_r = Position of the reference receiver.
- \mathbf{x}_i = Position of receiver i .
- t_r = Time of arrival for the reference receiver.
- t_i = Time of arrival for the receiver i .
- c = Speed of light.

To estimate the position of the transmitter system of equations 3.5 is solved [5]. The main challenge in implementing TDoA is synchronizing the clock in all receivers [25].

The TDoA system can be used in a variety of applications, such as indoor positioning, vehicle or people tracking, and asset tracking. The accuracy of the TDoA system depends on the number and placement of the UWB sensors and the timing resolution of the system.

■ Two-way ranging

Two-way ranging (TWR) is a technique used by UWB systems to estimate the distance between two devices. TWR requires two-way communication between two devices, where one device sends a signal to another device and waits for a response, as shown in figure 3.9. The time difference between the transmission and reception of the signal is used to calculate the distance between the two devices.

Single-sided two-way ranging (SS-TWR) is a technique where only one device sends a signal and waits for a response from another device. The time difference between the transmission and reception of the signal is used to calculate the distance between the two devices.

$$\text{TOF} = \frac{R_a - D_b}{2}$$

Where:

- TOF = Time of flight.
- R_a = Time of round trip
- D_b = Response delay.

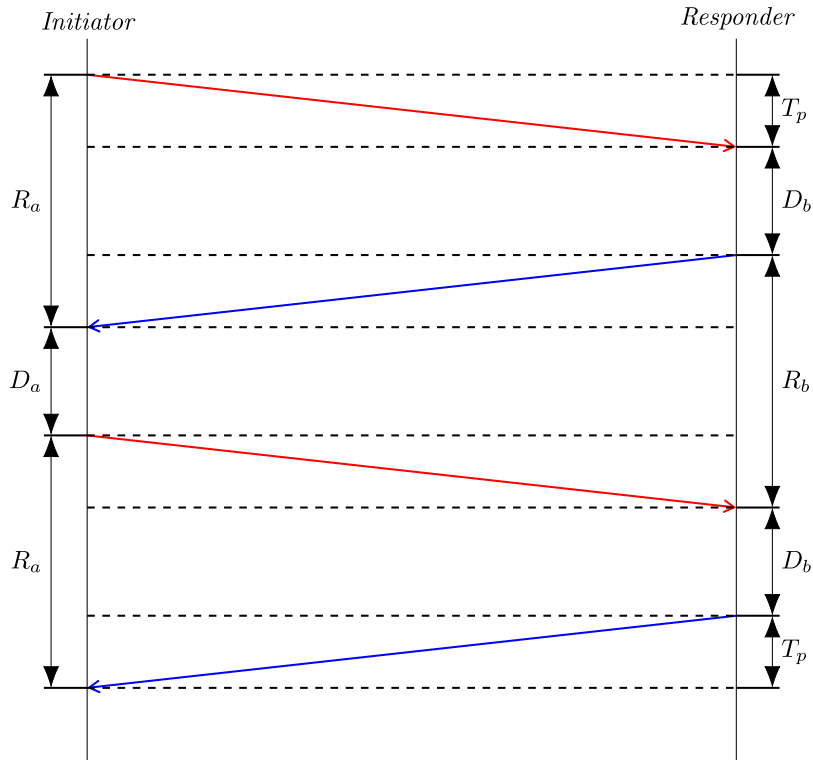


Figure 3.9: Two way ranging with two round trips.

Double-sided two-way ranging (DS-TWR) is a technique where both devices send signals and wait for responses from each other. The time difference between the transmission and reception of signals from both devices is used to calculate the distance between them.

$$\text{TOF} = \frac{R_a R_b - D_a D_b}{R_a + D_a + R_b + D_b}$$

The main advantage of DS-TWR is its ability to compensate for the effect of clock drift [3]. Clock drift refers to several related phenomena where a clock does not run at exactly the same rate as a reference clock. That is, after some time, the clock drifts apart or gradually desynchronizes from the other clock. All clocks are subject to drift, causing eventual divergence unless they are resynchronized. The drift of the clock can be caused by many factors, such as changes in temperature, aging of components, and changes in power supply voltage [3].



Chapter 4

Kalman filters

Kalman filters are a powerful mathematical technique that is used to estimate the state of a system from noisy measurements. Originally developed by Rudolf Kalman in 1960 [10], Kalman filters have become widely used in a variety of fields, including engineering, finance, and robotics. The Kalman filter is an optimal estimator, which means it provides the best estimate of the system state given the available measurements and knowledge of the dynamics of the system. The filter uses a state-space model of the system to predict the evolution of the system over time and to address measurement errors. The Kalman filter is particularly useful in applications where measurements are noisy or incomplete, or where the system dynamics are complex or difficult to model. In this way, the Kalman filter is an essential tool for many real-world applications that require accurate state estimation and control.

The algorithm involves two steps: prediction and update. The prediction step uses the previous state estimate and the dynamic model of the system to predict its current state and its uncertainty. The update step uses an obtained measurement and the measurement model of the system to correct the predicted state estimate and its uncertainty using a weighted average. The weight is determined by the Kalman gain, which balances the trust between the prediction and the measurement. The Kalman gain is computed on the basis of the covariance matrices of the prediction error and the measurement error. Prediction and update steps are performed recursively for each new measurement.

The linear Kalman filter assumes that the system and the measurement models are linear and can be represented by matrices. The extended Kalman filter extends the linear Kalman filter to handle non-linear systems by linearizing them around the current estimate using Taylor series expansion. The unscented Kalman filter improves the extended Kalman filter by using a set of sigma points to capture the mean and covariance of the nonlinear system without requiring linearization or Jacobian matrices [12,17]. The unscented

Kalman filter is more accurate and robust than the extended Kalman filter, especially for highly nonlinear systems [17] [24].

4.1 Linear Kalman filter

A linear Kalman filter is a recursive algorithm that uses the Bode-Shannon representation of random processes and the state-transition method of analysis of dynamic systems to estimate the state of a system from noisy measurements. In the prediction step 4.1, the algorithm uses a state transition matrix to project the current state and its covariance matrix to the next time step.

$$\begin{array}{l} \textit{Predict step} \\ \hline \hat{\mathbf{x}} = \mathbf{F}\mathbf{x} + \mathbf{B}\mathbf{u} \\ \hat{\mathbf{P}} = \mathbf{F}\mathbf{P}\mathbf{F}^T + \mathbf{Q} \end{array} \quad (4.1)$$

Where:

$$\begin{array}{l} \hat{\mathbf{x}}, \hat{\mathbf{P}} = \text{State mean and covariance} \\ \mathbf{F} = \text{Transition matrix} \\ \mathbf{Q} = \text{Process matrix} \\ \mathbf{B}, \mathbf{u} = \text{Input to the system} \end{array}$$

In the correction step 4.4, the algorithm uses a measurement matrix to update the predicted state and its covariance matrix with the new measurement. The algorithm optimizes the estimation by minimizing the mean squared error between the true state and the estimated state [10].

$$\begin{array}{l} \textit{Update step} \\ \hline \mathbf{y} = \mathbf{z} - \mathbf{H}\mathbf{x} \\ \mathbf{K} = \mathbf{P}\mathbf{H}^T(\mathbf{H}\mathbf{P}\mathbf{H}^T + \mathbf{R})^{-1} \\ \hat{\mathbf{x}} = \mathbf{x} + \mathbf{K}\mathbf{y} \\ \hat{\mathbf{P}} = (\mathbf{I} - \mathbf{K}\mathbf{H})\mathbf{P} \end{array} \quad (4.2)$$

Where:

$$\begin{array}{l} \mathbf{z}, \mathbf{R} = \text{Measurement and covariance} \\ \mathbf{H} = \text{Measurement function} \end{array}$$

4.2 Extended Kalman filter

The Kalman filter is an optimal estimation algorithm that combines measurements from sensors with predictions from a mathematical model to estimate the true state of a system. However, the Kalman filter assumes that both the system dynamics and the measurement model are linear. In real-world applications, many systems exhibit non-linear behavior, and the extended Kalman filter is used to handle such cases.

$$\begin{array}{l}
 \textit{Predict step} \\
 \hline
 \mathbf{F} = \left. \frac{\partial f(\mathbf{x}_t, \mathbf{u}_t)}{\partial \mathbf{x}} \right|_{\mathbf{x}_t, \mathbf{u}_t} \\
 \hat{\mathbf{x}} = f(\mathbf{x}, \mathbf{u}) \\
 \hat{\mathbf{P}} = \mathbf{F}\mathbf{P}\mathbf{F}^T + \mathbf{Q}
 \end{array} \tag{4.3}$$

The extended Kalman filter linearizes the system and measurement models using Taylor series expansions. It uses the first-order derivatives (Jacobian matrices) to linearize the equations $f(x)$ at each time step. The filter then performs the standard Kalman filter prediction and update steps using these linearized models.

$$\begin{array}{l}
 \textit{Update step} \\
 \hline
 \mathbf{H} = \left. \frac{\partial h(\mathbf{x}_t)}{\partial \mathbf{x}} \right|_{\mathbf{x}_t} \\
 \mathbf{y} = \mathbf{z} - h(\mathbf{x}) \\
 \mathbf{K} = \mathbf{P}\mathbf{H}^T(\mathbf{H}\mathbf{P}\mathbf{H}^T + \mathbf{R})^{-1} \\
 \hat{\mathbf{x}} = \mathbf{x} + \mathbf{K}\mathbf{y} \\
 \hat{\mathbf{P}} = (\mathbf{I} - \mathbf{K}\mathbf{H})\mathbf{P}
 \end{array} \tag{4.4}$$

It's worth noting that the extended Kalman filter has some limitations. Since it uses linear approximations, it may not perform well for highly non-linear systems or when the linearization is inaccurate [11]. In such cases, other techniques, such as the unscented Kalman filter or particle filters, may be more appropriate.

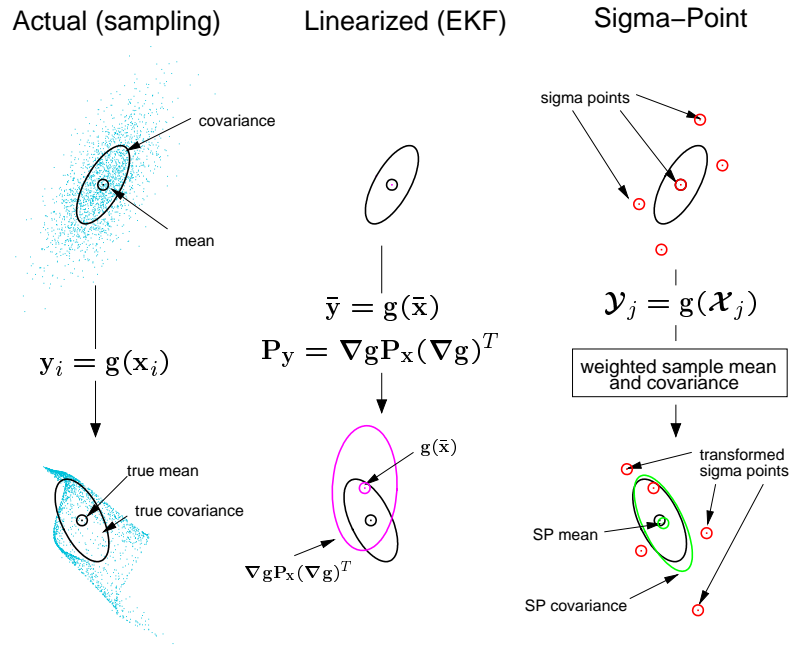


Figure 4.1: Comparison between sampling, EKF and sigma points. [13]

4.3 Unscented Kalman filter

The unscented Kalman filter (UKF) is a technique for nonlinear estimation that uses a deterministic sampling approach to propagate a Gaussian random variable through system dynamics [24]. The UKF employs the unscented transform (UT), which generates a set of sample points that capture the mean and covariance of the original distribution.

The unscented transform is a technique for approximating the outcome of applying a nonlinear function to a probability distribution that is described by a mean and a covariance matrix. It does this by choosing a set of points, known as sigma points Figure 4.1.

Merwe describes generating the sigma points in the paper *The unscented Kalman filter for nonlinear estimation*[24]. These sigma points are chosen to capture the mean and covariance of the current estimated state and are transformed through the non-linear model to predict the state at the next time step. The sigma points \mathcal{X}_i as well as the weights ω_i for each point are calculated using equation 4.5. The weights ω_i must follow the equation $\sum_{i=0}^{2L} \omega_i = 1$.

$$\lambda = \alpha^2(L + \kappa) - L$$

$$\begin{aligned} \mathcal{X}_0 &= \hat{x} & \omega_0^m &= \frac{\lambda}{L + \lambda} & i &= 0 \\ \mathcal{X}_i &= \hat{x} + \left(\sqrt{(L + \lambda)\mathbf{P}_x} \right)_i & \omega_i^c &= \frac{1}{2(L + \lambda)} + (1\alpha^2 + \beta) & i &= 1, \dots, L \\ \mathcal{X}_i &= \hat{x} - \left(\sqrt{(L + \lambda)\mathbf{P}_x} \right)_i & \omega_i^m &= \omega_i^c = \frac{1}{2(L + \lambda)} & i &= L + 1, \dots, 2L \end{aligned} \quad (4.5)$$

Where:

$$\begin{aligned} \hat{\mathbf{x}}, \mathbf{P}_x &= \text{State vector and covariance} \\ L &= \text{Dimension of state vector} \\ 0 &\leq \alpha \leq 1 \\ 0 &\leq \kappa \\ 0 &\leq \beta \end{aligned}$$

The sigma points are used both in the predict step 4.6 and update step 4.7 and need to be regenerated for each new measurement. Instead of the matrix \mathbf{F} 4.1 and \mathbf{H} 4.4 known from LKF, the UKF is provided with non-linear functions $\mathbf{f}(\mathcal{X})$ and $\mathbf{h}(\mathcal{X})$.

$$\begin{aligned} &\text{Predict step} \\ \hline &\mathcal{Y} = \mathbf{f}(\mathcal{X}) \\ \hat{\mathbf{x}} &= \sum_{i=0}^{2L} \omega_i^m \mathcal{Y}_i & \hat{\mathbf{P}} &= \sum_{i=0}^{2L} \omega_i^c (\mathcal{Y}_i - \mathbf{x})(\mathcal{Y}_i - \mathbf{x})^T + \mathbf{Q} \end{aligned} \quad (4.6)$$

By comparing the predicted measurements with the actual measurements, the UKF computes the Kalman gain, which determines the optimal blend between the predicted state and the measurement updates. Finally, the updated state estimate is obtained by incorporating the measurement information into the predicted state estimate using the Kalman gain. The update step of the UKF enables the filter to adaptively adjust the state estimate based on the measurements, providing a more accurate estimation of the true state of the system.

$$\begin{aligned}
& \text{Update step} \\
& \hline
& \mathbf{Z} = \mathbf{h}(\boldsymbol{\mathcal{X}}) \\
\mu_z &= \sum_{i=0}^{2L} \omega_i^m \mathbf{Z}_i & \mathbf{P}_z &= \sum_{i=0}^{2L} \omega_i^c (\mathbf{Z}_i - \mu_z)(\mathbf{Z}_i - \mu_z)^T + \mathbf{R} \\
\mathbf{y} &= \mathbf{z} - \mu_z & \mathbf{P}_{xz} &= \sum_{i=0}^{2L} \omega_i^c (\boldsymbol{\mathcal{X}}_i - \mathbf{x})(\mathbf{Z}_i - \mu_z)^T \\
& & \mathbf{K} &= \mathbf{P}_{xz} \mathbf{P}_z^{-1} \\
\hat{\mathbf{x}} &= \mathbf{x} + \mathbf{K}\mathbf{y} & \hat{\mathbf{P}} &= \mathbf{P} - \mathbf{K}\mathbf{P}_z\mathbf{K}^T
\end{aligned} \tag{4.7}$$

The UKF has been shown to achieve higher accuracy and robustness than the extended Kalman filter (EKF) for various non-linear estimation problems, such as state estimation, parameter estimation, and dual estimation [24].

Chapter 5

UAV implementation

The proposed measurement system is designed to work with the existing MRS UAV System that has been developed by the MRS group at CTU. The MRS system relies on the use of the Robot Operating System (ROS) in version ROS Noetic released in 2020¹.

ROS is a robust framework that is used to develop and control robots. It provides a variety of tools and libraries that make the development of robot software easier. ROS uses a distributed system, allowing different parts of a robot to communicate with each other using a messaging model. It supports multiple programming languages, making it accessible to developers. ROS has a large community and a wide range of preexisting packages, making it a popular choice for research and industrial applications.

An overview of the proposed system is shown in figure 5.1. This thesis implements the blue-colored blocks, and these blocks will be explained in more detail in this chapter.

5.1 Qorvo DW1000 UWB PHY radio

Qorvo DW1000 is a UWB PHY radio developed and manufactured by Qorvo². The proposed solution utilizes a Qorvo DWM1001-DEV development board which consists of a DWM1001C transceiver module and a J-Link debug probe. Figure 5.2 showcases the printed circuit board (PCB) of the Qorvo DWM1001-DEV. The DWM1001C houses the DW1000 radio chip, nRF52832 microcontroller, 3.0 V, and 1.8 V power supplies. The DW1000 is connected

¹ROS Noetic release info <http://wiki.ros.org/noetic>

²Qorvo DW1000 <https://www.qorvo.com/products/p/DW1000>

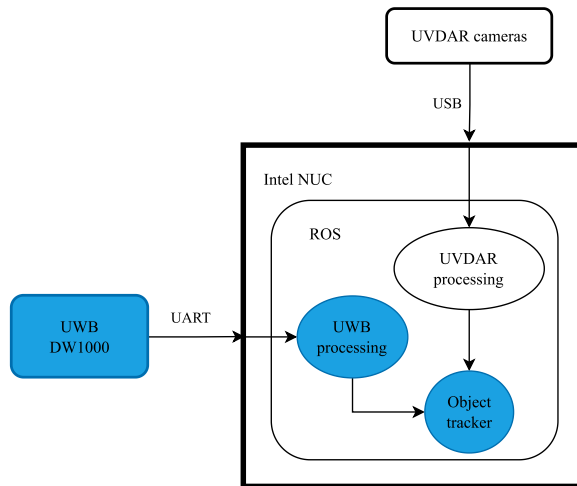


Figure 5.1: System overview.

to the nRF52832 via the SPI bus. The module also includes Bluetooth connectivity and an accelerometer, but it remained unutilized.

The nRF52832 is the microcontroller that gets programmed. The programming language of choice is C++ with combination of Zephyr RTOS³ which enables use of multitasking and concurrency. Zephyr RTOS also contains a rich selection of peripheral drivers for faster development and higher abstraction.

A ranging technique of choice is double-sided two-way ranging. It fulfills all the needs, as it compensates for clock drift and does not require any infrastructure. Each of the two devices in the ranging instance fills out fields in the ranging message 5.3. The values in the ranging message are referenced to DW1000 clock frequency. Therefore, in order to get an actual time, the values need to be multiplied by 15.65 ps. The solution has the ability to measure in *many-to-many* forming a complete graph.

Data from UWB are sent to ROS via UART connection at baud rate 115200. As a communication protocol, the Baca Protocol is used as recommended by the MRS group⁴.

UWB ranging on the ROS side handles `uwb_range_node`. The node decodes the messages and republishes them as ROS topics. Every N seconds, the node sends a beacon message through the UWB. This message is then received and processed by other UAVs. An essential function of the beacon

³Zephyr RTOS <https://zephyrproject.org/>

⁴Baca protocol https://github.com/ctu-mrs/mrs_serial

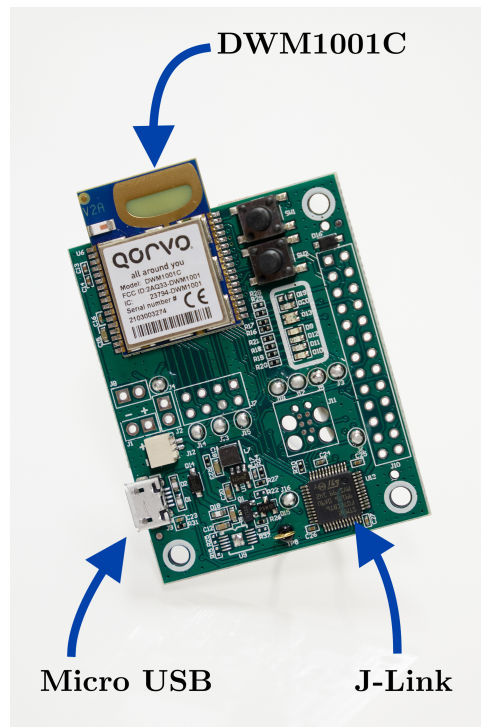


Figure 5.2: Qorvo DWM1001 development board.

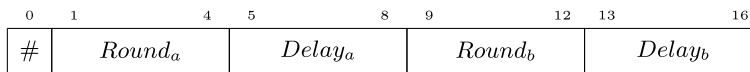


Figure 5.3: Structure of ranging message. Numbers denote bytes.

message is to synchronize the UWB measurements with UVDAR measurements, enabling the fusion of the measurements based on IDs. This is done via the UAV identifier that is embedded in the beacon message. The retrieved ID from the beacon message is assigned to the MAC addresses in the address resolution table.

■ 5.2 Object tracker

An object tracker is an ROS node where the measurements are fused. Both linear and unscented Kalman filters are utilized in this node, as can be seen in figure 5.4. The fuse proceeds in the world frame to negate the effects of ego-motion.

For the predict step, an implementation from LKF is used with the state

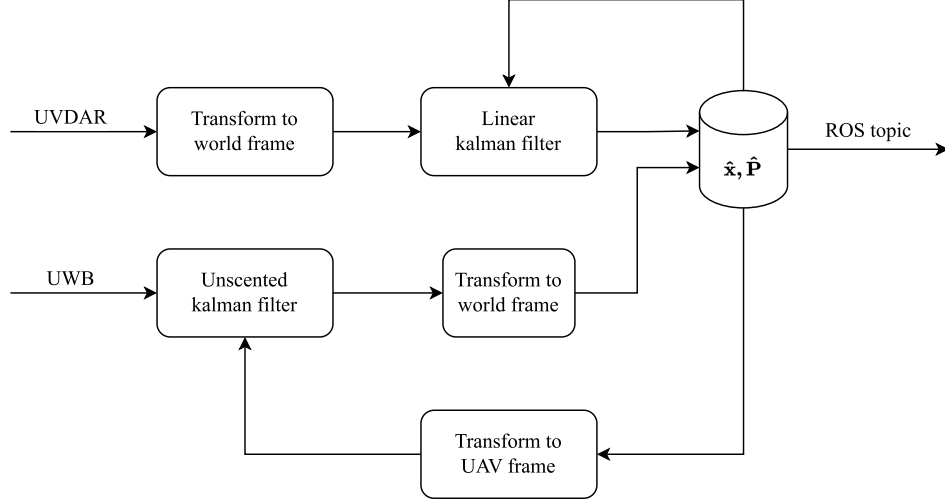


Figure 5.4: Fuse of UVDAR and UWB measurements using Kalman filters.

vector and transition matrix described by equations 5.1.

$$\mathbf{x} = [x \ y \ z \ roll \ pitch \ yaw]^T$$

$$\mathbf{F} = \begin{bmatrix} 1 & 0 & 0 & 0 & 0 & 0 \\ 0 & 1 & 0 & 0 & 0 & 0 \\ 0 & 0 & 1 & 0 & 0 & 0 \\ 0 & 0 & 0 & 1 & 0 & 0 \\ 0 & 0 & 0 & 0 & 1 & 0 \\ 0 & 0 & 0 & 0 & 0 & 1 \end{bmatrix} \quad (5.1)$$

Figure 5.5 depicts the challenge of integrating UWB and UVDAR.

The UVDAR measurement consists of a position described by Cartesian coordinates and orientation described by a quaternion as shown in 5.2 with a corresponding covariance matrix. The measurement is in the frame of the camera, but with help of `mrs_transformer` the coordinates are transformed to the world coordinates.

$$\text{position} = [x \ y \ z]^T \quad \text{orientation} = [x \ y \ z \ w]^T \quad (5.2)$$

For this kind of measurement, the linear Kalman filter is the best choice, because there are no nonlinearity functions and the computation cost is low. The rotation from UVDAR is transformed from quaternion to Euler angles. A measurement matrix \mathbf{H} is a simple identity matrix of dimension six.

The UWB measurement acquires the distance from UAV \mathbf{x}_1 to UAV \mathbf{x}_2 as noted in equation 5.3.

$$UWB_{distance} = \sqrt{(\mathbf{x}_2 - \mathbf{x}_1)^T (\mathbf{x}_2 - \mathbf{x}_1)} \quad (5.3)$$

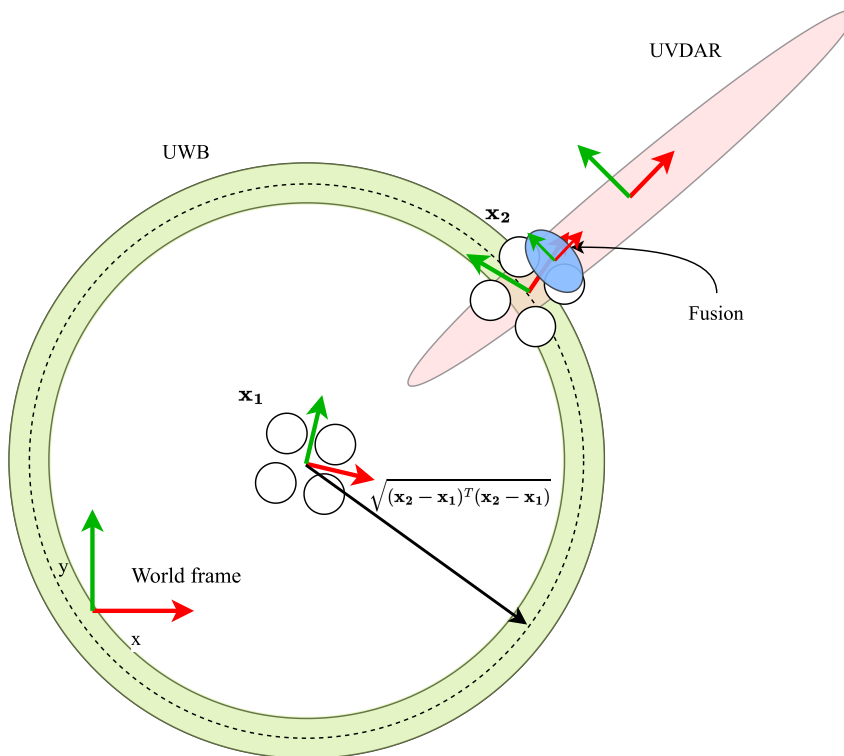


Figure 5.5: Situational schema of data fusion.

The problem is non-linear and requires a more complex approach. For this reason, the unscented Kalman filter is employed for fusing distance. The previous state needs to be transformed from world frame to UAV frame. The result needs to be transformed back to world frame back to world. The measurement function is described as a C++ function 5.6.

```

kalman::range_ukf_t::z_t observe_ukf(
    const kalman::range_ukf_t::x_t &x)
{
    Eigen::VectorXd pose(3);

    pose << x[(int)STATE::X],
           x[(int)STATE::Y],
           x[(int)STATE::Z];
    kalman::range_ukf_t::z_t z;

    z << pose.norm();
    return z;
}

```

Figure 5.6: Measurement function for fusing distance.

Chapter 6

Simulations and real-world experiments

A series of experiments have been conducted to evaluate the performance of the proposed measurement system. Experiments took place at Temešvár (N49.36225 E14.26143). A two Holybro X500 6.1 equipped with Qorvo DWM1000 has been chosen as a UAV platform. These drones were mainly chosen due to the RTK GNSS system onboard, which is crucial for evaluating accuracy by using them as a source of ground truth.

6.1 Ultra-wide band experiments

Line segment test

This experiment aims to test the maximum range and obtain a transfer characteristic of the sensor. The purpose of the first UAV was to act as an observer and, for the duration of the test remained at position $[0 \ 0 \ 5]^T$. The second UAV was flying on a trajectory predefined by the parametric equation 6.1.

$$\mathbf{position}(t) = \begin{bmatrix} 0 \\ 65 + 55 \sin(2\pi t) \\ 5 \end{bmatrix}, \quad t \in (0, 1) \quad (6.1)$$

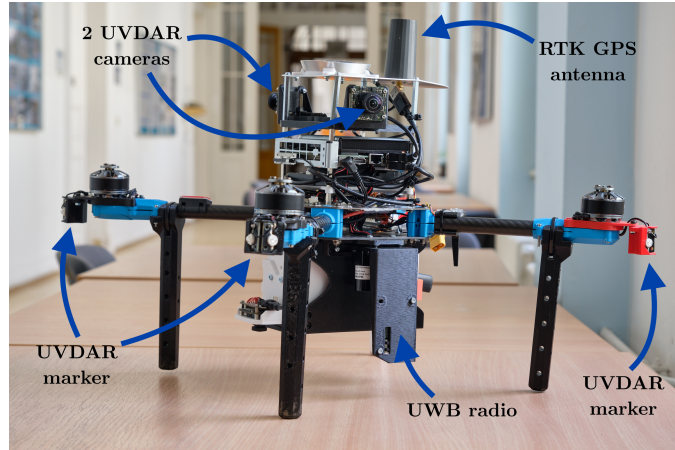


Figure 6.1: Holybro X500 with UVDAR cameras and UWB radio.

■ Circular trajectory

As noted above, the results from the UWB should be the same for all orientations. To test whether that is a correct assumption, 4 experiments have been conducted. In each test, one UAV acted as an observer and stayed at position $[0 \ 0 \ 5]^T$. The second UAV followed a circle of radius 10 m around the first UAV in a car-like motion. The difference between the 4 experiments was the relative angle θ as shown in figure 6.2.

■ Results

All proposed experiments regarding the UWB were successfully conducted. Results from the first experiment in Figure 6.3 showed that the UWB measurements are indeed precise and do not express any signs of nonlinearity. The maximum range of 120 m was reached by UWB, however, the measurements at the far end are not reliable and often drop out.

As Figure 6.5 shows, the measurement error is dependent on the angle. In *A sources of error in DW1000* [3] the manufacturer mentions that there are two sources of error, clock drift and received signal level. The implemented ranging technique (double-sided two-way ranging) compensates for clock drift. Therefore, the only error source left is the received signal level. The more powerful the signal, the sooner it is timestamped, leading to a shorter distance reported. This error could be easily corrected by constructing correction function $f(\text{dB})$. Unfortunately, the received signal level was not recorded.

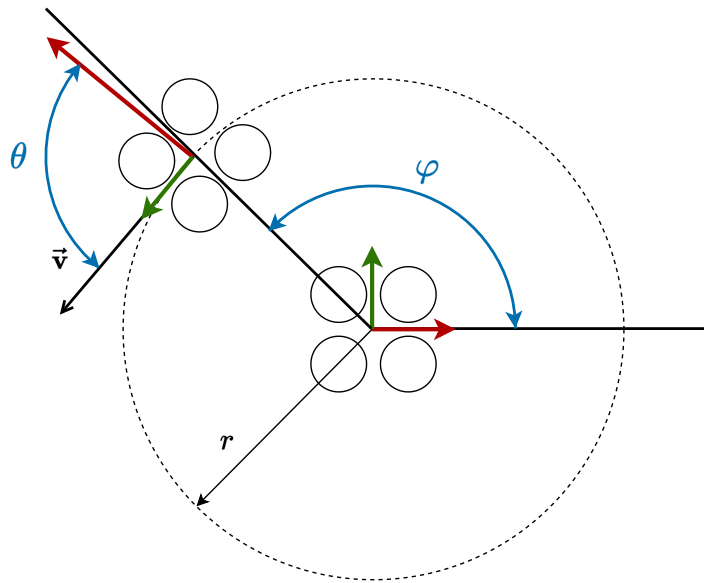


Figure 6.2: Circular trajectory experiment.

Further research should be done to correct errors dependent on the level of the received signal.

Results and ranging multiple static responders with UWB is demonstrated in Appendix C.

6.2 UVDAR and UWB fusion experiments

Leader follower algorithm

To test the fusion of UVDAR and UWB in loop, a leader-follower algorithm was used. In this test, a leader UAV flies a pre-planned trajectory. A follower UAV tries to follow the leader based only on UVDAR and UWB sensor fusion. The algorithm was inspired by the *UVDAR System for Visual Relative Localization With Application to Leader-Follower Formations of Multirotor UAVs* [21] and is represented in figure 6.6. The follower was set to follow the leader with $r = 6$ m and $\varphi = 180^\circ$.

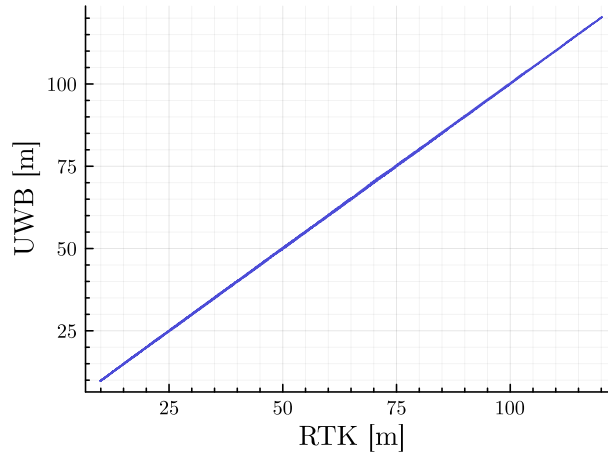


Figure 6.3: Transfer characteristic of UWB.

■ Results

Unfortunately, due to an incorrect configuration of the experiment, the test has not been successfully conducted in real-life. A simulated test using the Gazebo simulator¹ was conducted as an alternative approach. A special node was made to simulate results from UWB, the node calculates a distance between UAVs from ground truth and then adds noise with distribution $\mathcal{N}(0, 0.05)$. The test was repeated two times. First, the UWB and UVDAR fusion was kept for the whole time, providing an accurate position of the leader UAV. During the second test, the fusion process was halted mid-way and only UVDAR measurements were utilized.

The results depicted in Figure 6.7 demonstrate the advantages of fusing the UWB and UVDAR technologies. Due to the absence of precise distance measurements from UWB (Ultra-Wideband) technology, the follower UAV could not maintain track of the leader UAV.

More simulated tests of the Object tracker can be seen in Appendix C.

¹Gazebo simulator <https://gazebosim.org/home>

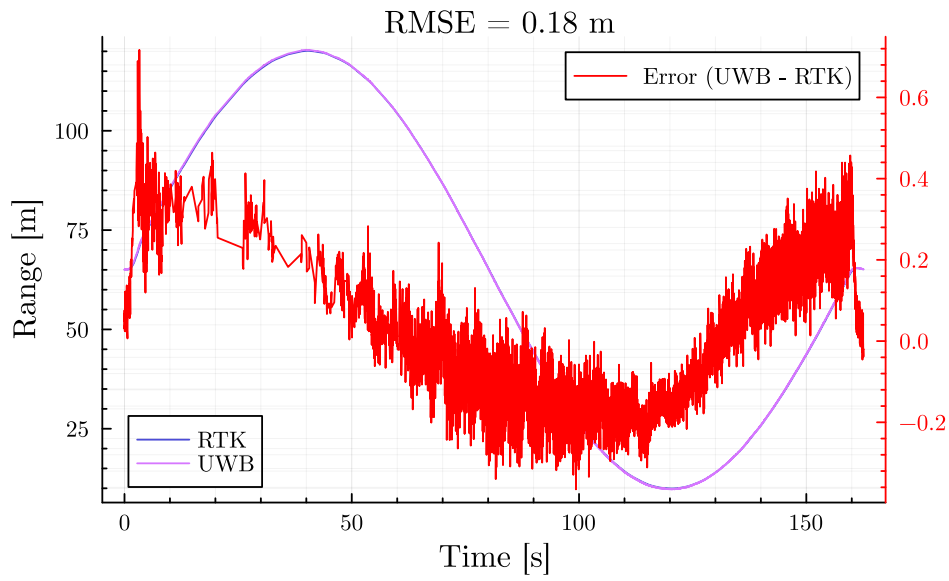


Figure 6.4: Trajectory plotted in time with error.

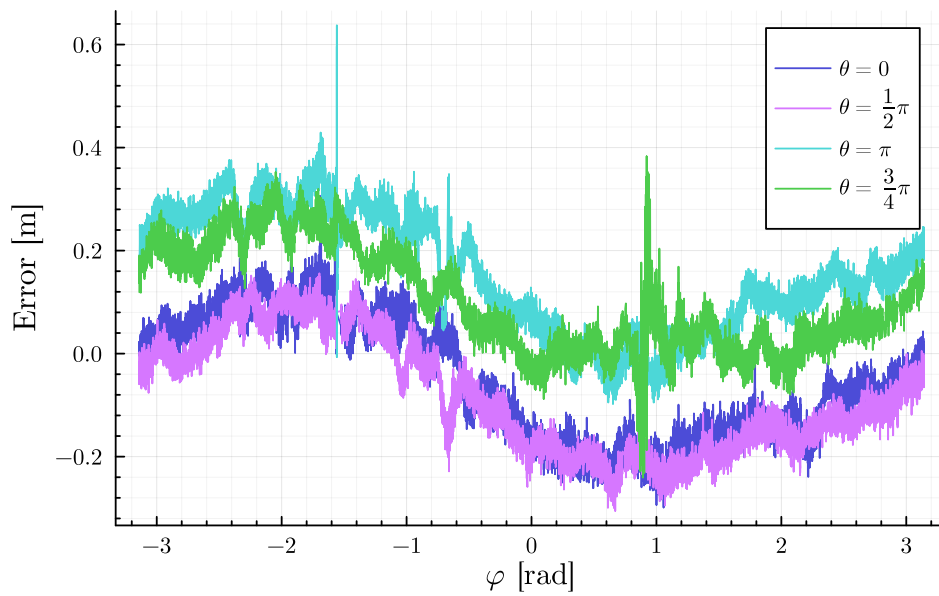


Figure 6.5: Comparison between different radiation angles.

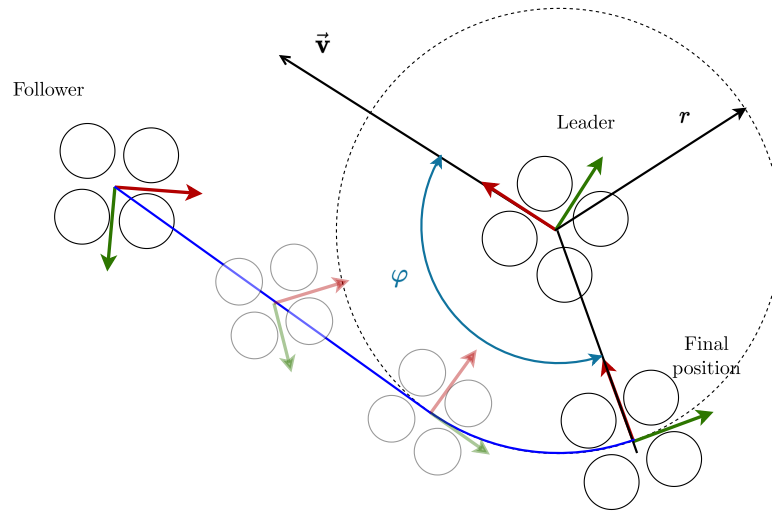


Figure 6.6: Visual representation of the leader-follower algorithm.

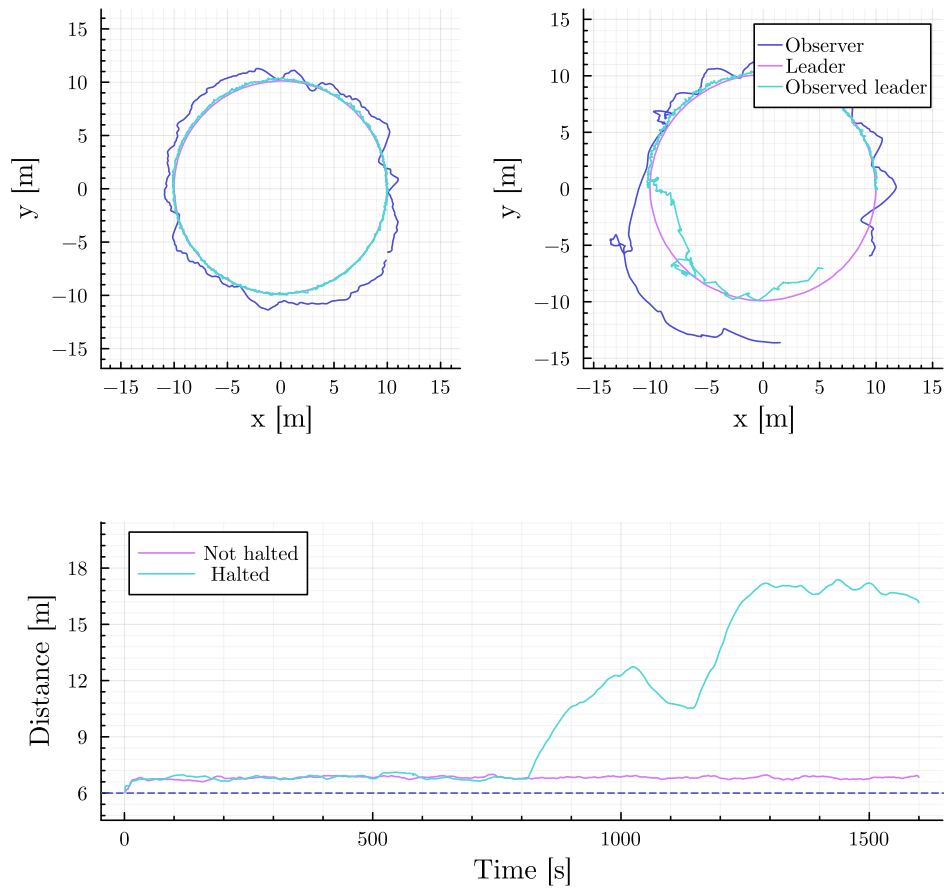



Figure 6.7: Leader-follower algorithm results.



Chapter 7

Conclusion

In conclusion, this thesis has made significant contributions to the enhancement of visual relative mutual localization systems, particularly in the context of UAV swarms. The primary focus was to improve accuracy and reliability by integrating Ultra-wide band (UWB) technology for distance measurements.

The proposed solution utilized the Qorvo DWM1000 UWB radio as a means of acquiring distance measurements. The firmware designed for the UWB radio utilizes a distributed many-to-many ranging approach employing double-sided two-way ranging. The Object tracker ROS node was developed to facilitate the fusion of UVDAR and UWB data by leveraging the mathematical framework of Kalman filters. This fusion approach has demonstrated its versatility, as it can be applied not only to mutual localization within UAV swarms but also to localize unmanned ground vehicles (UGVs) or serve as a navigation beacon for landing platforms.

Although the current implementation of UWB has shown reliable performance, there is room for further improvement. Future work should focus on refining the UWB implementation to correct errors caused by variations in received signal levels. Additionally, the utilization of advanced UWB radios with 3D localization capabilities, employing antenna arrays, could enable the deployment of redundant systems onboard UAVs, further enhancing accuracy and robustness.

The results of this thesis have contributed significantly to the ecosystem of the MRS group, providing researchers with a high-precision relative mutual localization system. By extending the boundaries of what is possible, this system opens up new avenues for research and exploration in various domains.

The developed system holds immense potential for a wide range of appli-

cations, from collaborative tasks and swarm coordination in UAV swarms to autonomous navigation and precise landing capabilities. The integration of UVDAR and UWB technology has paved the way for advancements in the field, enabling researchers to push the boundaries of what can be achieved with UAV swarms and other autonomous systems.

In conclusion, this thesis has successfully addressed the challenges associated with visual relative mutual localization in UAV swarms by integrating UWB technology. The proposed fusion approach and its future potential have made valuable contributions to the field, providing researchers with the means to expand the possibilities of UAV swarm applications.



References

1. 2003. ATPL: Radio navigation.
2. 2011. IEEE standard for local and metropolitan area networks–part 15.4: Low-rate wireless personal area networks (LR-WPANs). *IEEE Std 802.15.4-2011 (Revision of IEEE Std 802.15.4-2006)*: 1–314. <https://doi.org/10.1109/IEEESTD.2011.6012487>
3. 2014. *A sources of error in DW1000 based two-way ranging scheme APS011*. Decawave; <https://www.qorvo.com/products/d/da008446>.
4. 2016. IEEE standard for low-rate wireless networks. *IEEE Std 802.15.4-2015 (Revision of IEEE Std 802.15.4-2011)*: 1–709. <https://doi.org/10.1109/IEEESTD.2016.7460875>
5. 2021. *Object tracking using time difference of arrival*. MathWorks; <https://www.mathworks.com/help/fusion/ug/object-tracking-using-time-difference-of-arrival.html>.
6. 2021. *European GNSS contingency/revision handbook for PBN operations: PBN handbook no. 6*. Eurocontrol, Brussels.
7. 2022. ACAS guide: Airborne collision avoidance systems.
8. CAE Oxford Aviation Academy. 2014. *Radionavigation: ATPL ground training series*. CAE Oxford Aviation Academy, United Kingdom.
9. Shuqiang Cao, Yongbin Zhou, Dong Yin, and Jun Lai. 2018/03. UWB based integrated communication and positioning system for multi-UAVs close formation. In *Proceedings of the 2018 international conference on mechanical, electronic, control and automation engineering (MECAE 2018)*, 475–484. <https://doi.org/10.2991/mecae-18.2018.98>
10. R. E. Kalman. 1960. A New Approach to Linear Filtering and Prediction Problems. *Journal of Basic Engineering* 82, 1: 35–45. <https://doi.org/10.1115/1.3662552>

22. V. Walter, N. Staub, M. Saska, and A. Franchi. 2018. Mutual localization of UAVs based on blinking ultraviolet markers and 3D time-position through transform. In *14th IEEE international conference on automation science and engineering (CASE 2018)*.
23. V. Walter, M. Saska, and A. Franchi. 2018. Fast mutual relative localization of UAVs using ultraviolet LED markers. In *2018 international conference on unmanned aircraft system (ICUAS 2018)*.
24. E. A. Wan and R. Van Der Merwe. 2000. The unscented Kalman filter for nonlinear estimation. In *Proceedings of the IEEE 2000 adaptive systems for signal processing, communications, and control symposium (cat. no. 00EX373)*, 153–158. <https://doi.org/10.1109/ASSPCC.2000.882463>
25. Yan Xie, Gerard J. M. Janssen, and Alle-Jan van der Veen. 2016. A practical clock synchronization algorithm for UWB positioning systems. In *2016 IEEE international conference on acoustics, speech and signal processing (ICASSP)*, 3891–3895. <https://doi.org/10.1109/ICASSP.2016.7472406>
26. Hao Xu, Luqi Wang, Yichen Zhang, Kejie Qiu, and Shaojie Shen. 2020. Decentralized visual-inertial-UWB fusion for relative state estimation of aerial swarm. In *2020 IEEE international conference on robotics and automation (ICRA)*, 8776–8782. <https://doi.org/10.1109/ICRA40945.2020.9196944>
27. Wenda Zhao, Abhishek Goudar, and Angela P. Schoellig. 2022. Finding the right place: Sensor placement for UWB time difference of arrival localization in cluttered indoor environments. *IEEE Robotics and Automation Letters* 7, 3: 6075–6082. <https://doi.org/10.1109/LRA.2022.3165181>

Appendix A

Source code

The attached zip file contains all the source codes, which can also be found in a GitHub repository.

List of source codes:

- leader-follower
ROS node that implements the leader-follower algorithm.
- Object-tracker-ROS
ROS node for UWB and UVDAR data fusion. Could be used for other types of position/distance sensors as well.
- UWB_MRS_ranging_ros_node
ROS node for communication with DWM1001-DEV.
- UWB-MRS-ranging
Zephyr RTOS application for DWM1001. The nRF Connect SDK is needed for compilation and flashing.
- UWB-workspace
Complete ROS Noetic workspace for UWB. Includes all necessary packages with real-world tmux scripts and gazebo simulations.

The source code for the thesis is at <https://github.com/vitpetrik/UWB-thesis> and can be viewed as a web page at <https://vitpetrik.github.io/UWB-thesis/>.

All the source codes are tested on Ubuntu 20.04 and should compile right away. In case of any trouble, feel free to contact the author of this thesis at petrivi2@fel.cvut.cz, vit.petrik@gmail.com, or GitHub.

Appendix B

ISO-OSI network model

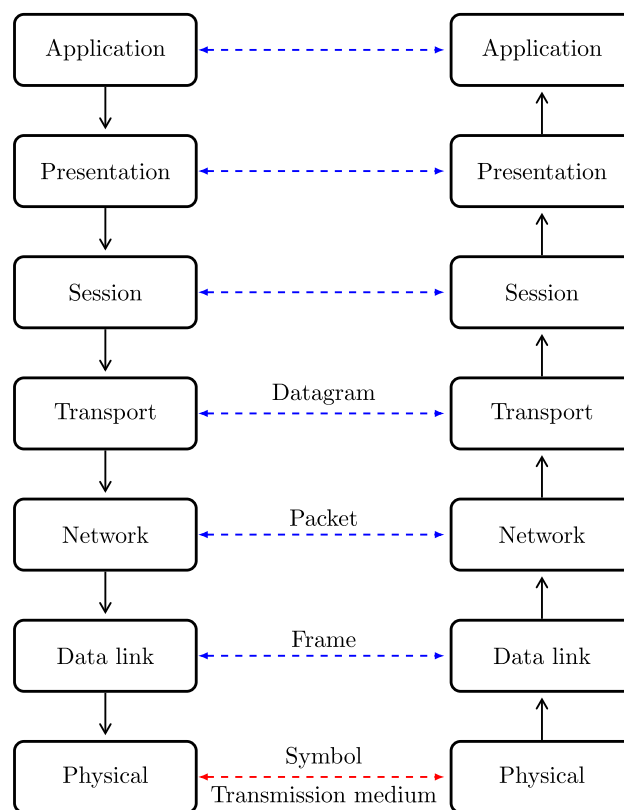


Figure B.1: OSI-ISO network model.

Appendix C

Object tracker and UWB evaluation tests

Multiple tests were run to evaluate the function of the Object tracker. As a test environment, the Gazebo simulator was used. The first UAV, an observer, remained at the coordinates $[0 \ 0 \ 5]^T$ for the entire duration of the tests. The second UAV, a performer, followed a pre-planned trajectory.

Range error is the difference between the ground truth distance between the UAVs and the distance calculated via unscented transform from Object tracker pose estimation.

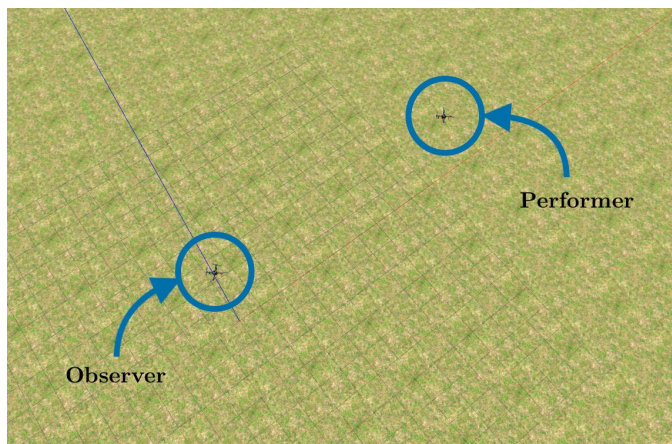
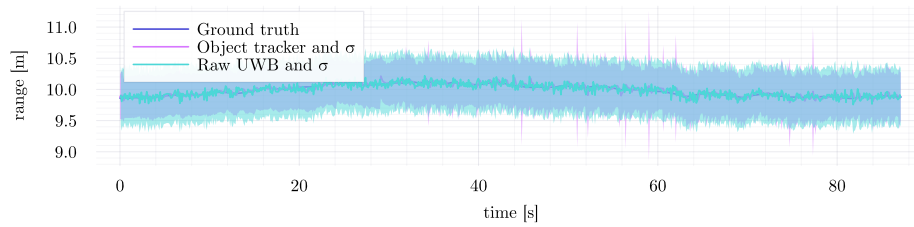


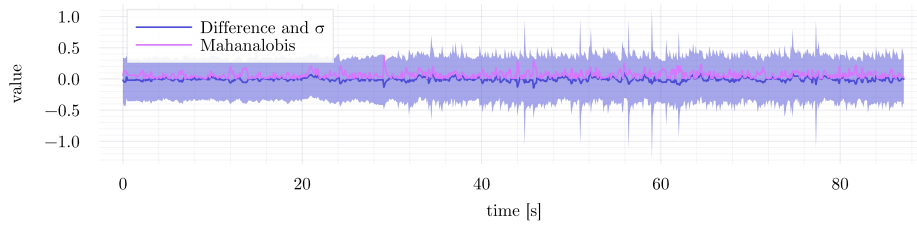
Figure C.1: Screenshot from Gazebo simulator showing the two UAVs.

RMSE = 0.92, MAE = 0.77

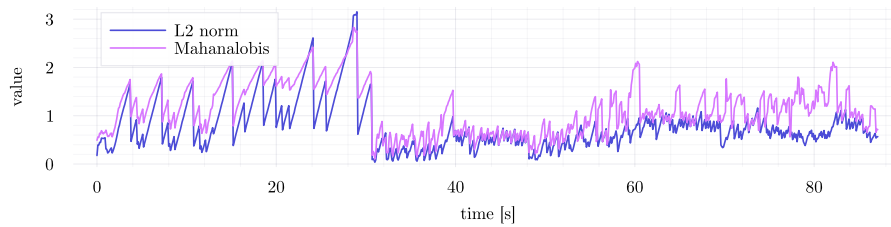
Range



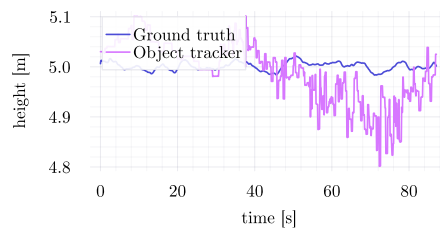
Range error



Position error



Height



Trajectory

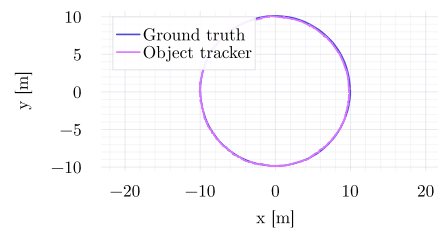


Figure C.2: Circle path with UWB fusion.



Figure C.3: Circle path with standalone UVDAR.

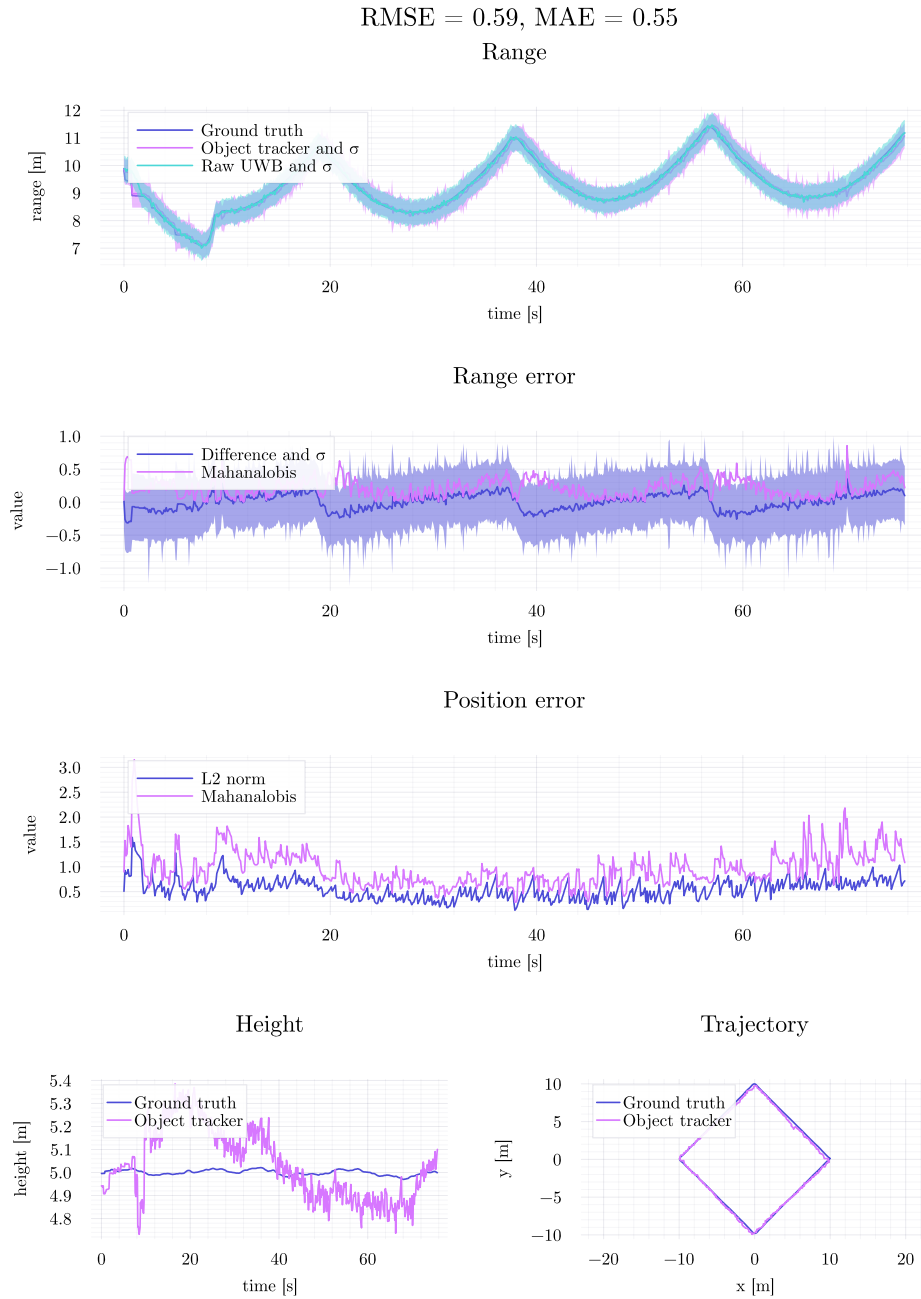


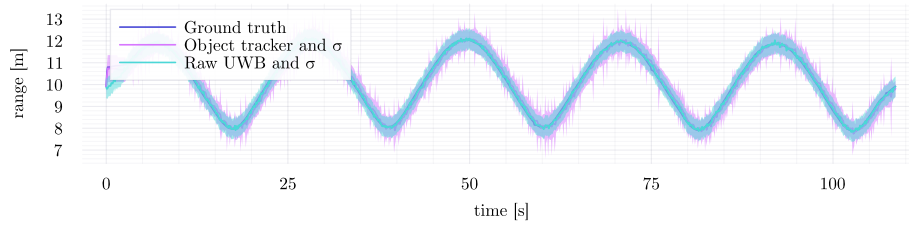
Figure C.4: Square path with UWB fusion.



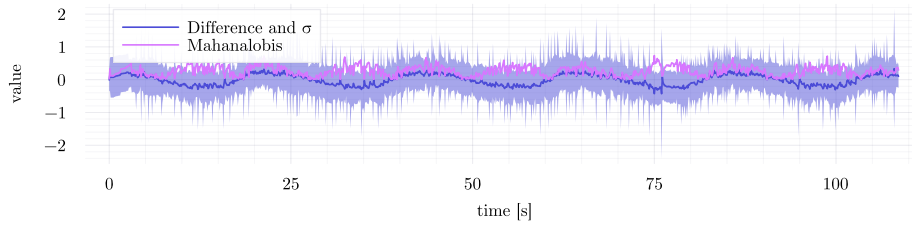
Figure C.5: Square path with UWB fusion.

RMSE = 0.81, MAE = 0.77

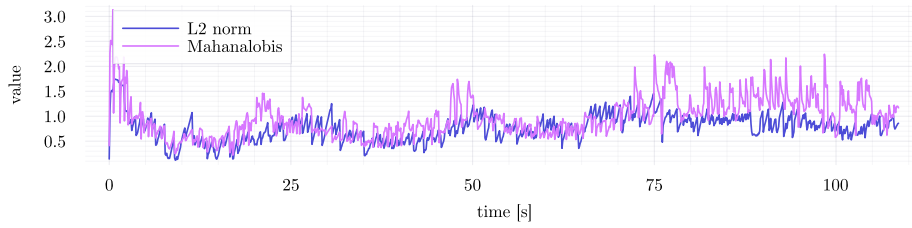
Range



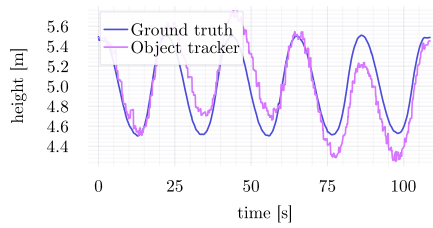
Range error



Position error



Height



Trajectory

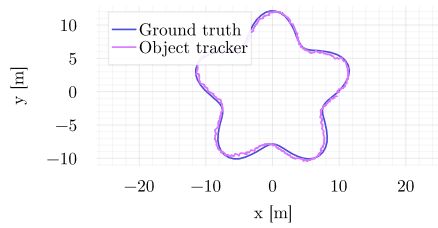


Figure C.6: Flower path with UWB fusion.

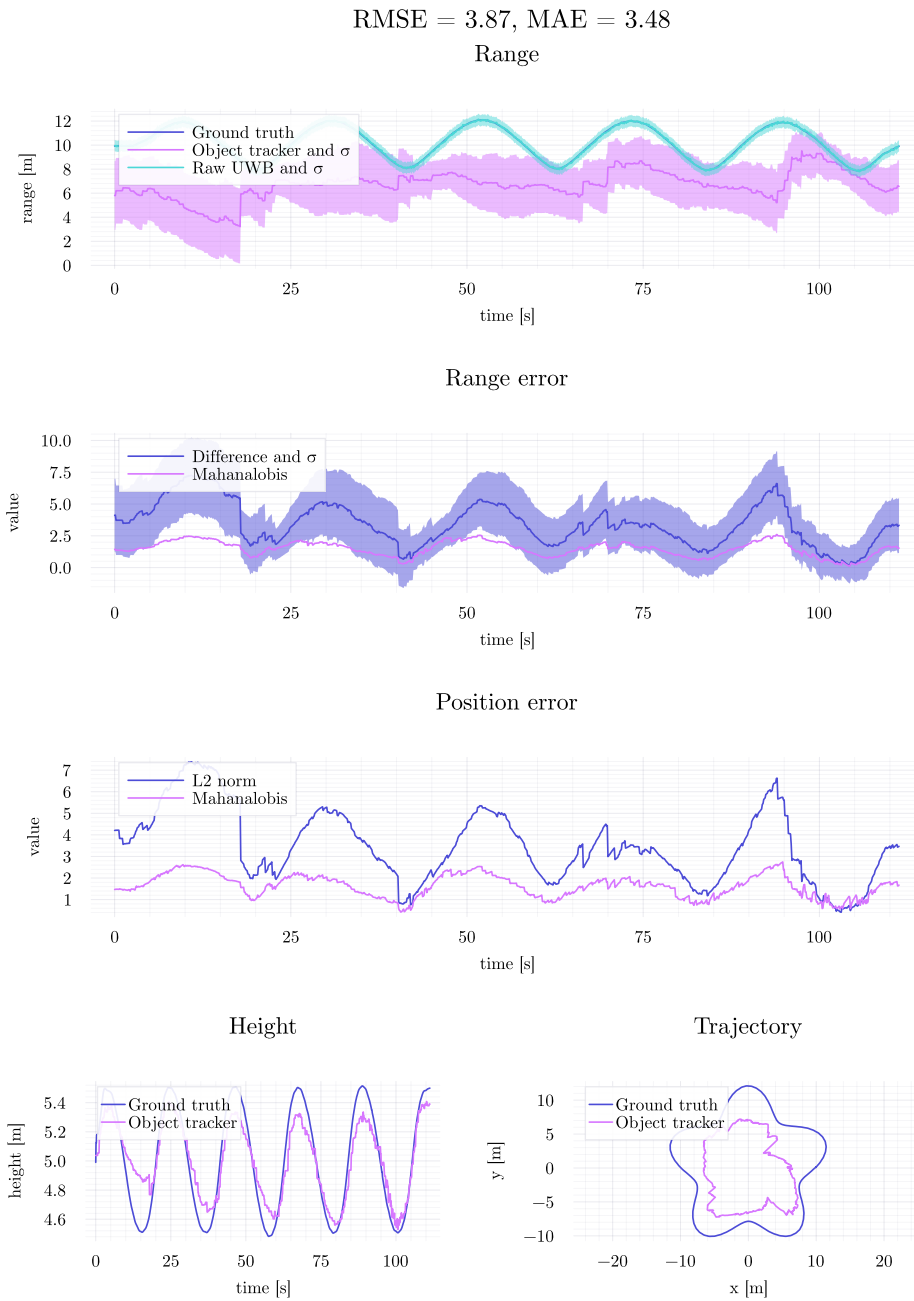


Figure C.7: Flower path with standalone UVDAR.

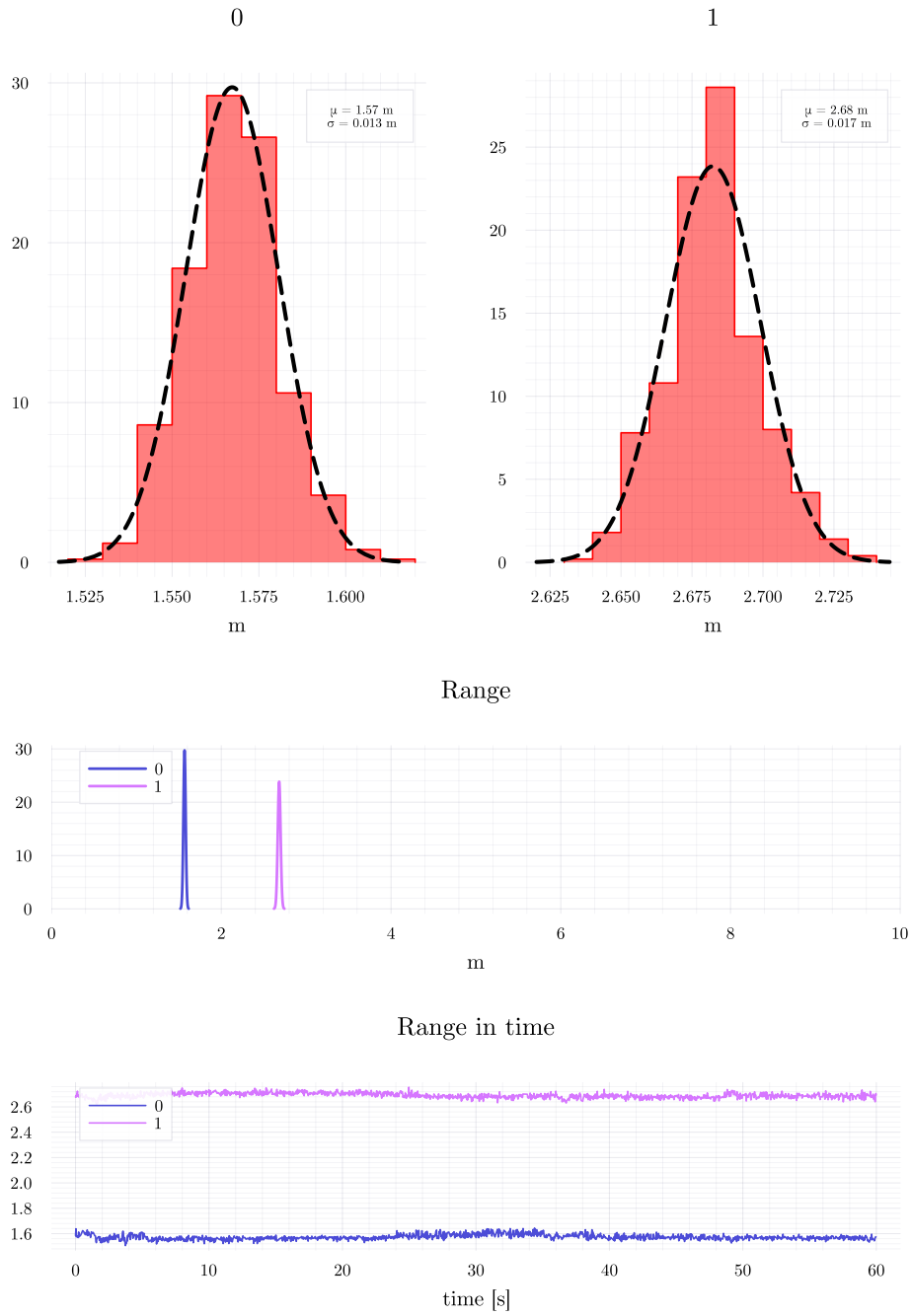


Figure C.8: Test of not moving UWBs.